Evaluation of High-Precision, Single-Frequency GPS Point Positioning Models

Tomas Beran[1], Sunil B. Bisnath[2] and Richard B. Langley[1]

[1] *Geodetic Research Laboratory, Department of Geodesy and Geomatics Engineering*
University of New Brunswick, Fredericton, New Brunswick, Canada
[2] *Harvard-Smithsonian Center for Astrophysics, Cambridge, Massachusetts, USA*

BIOGRAPHY

Tomas Beran received his Master's degree in surveying science from the Czech Technical University in Prague in 1999. He is currently a Ph.D. candidate in the Department of Geodesy and Geomatics Engineering at the University of New Brunswick (UNB), where he is investigating the use of GPS for single-frequency precise point positioning. This research is being performed under the supervision of Professor Richard Langley at the department's Geodetic Research Laboratory.

Sunil Bisnath is a geodesist at the Harvard-Smithsonian Center for Astrophysics in Cambridge, Massachusetts, where his responsibilities include management of the BARGEN geodetic network. Previously, Dr. Bisnath worked as a GPS research scientist at the Hydrographic Science Research Center at the University of Southern Mississippi. He received an Honours B.Sc. in 1993 and M.Sc. in 1995 in surveying science from the University of Toronto and a Ph.D. from the University of New Brunswick in 2004.

Richard Langley is a professor in the Department of Geodesy and Geomatics Engineering at the University of New Brunswick, where he has been teaching and conducting research since 1981. He has a B.Sc. in applied physics from the University of Waterloo and a Ph.D. in experimental space science from York University, Toronto. Professor Langley has been active in the development of GPS error models since the early 1980s and is a contributing editor and columnist for GPS World magazine. He is a fellow of the Institute of Navigation (ION) and shared the ION Burka Award for 2003.

ABSTRACT

In this paper we evaluate the performance of single-frequency, single-point positioning processors with an emphasis on ionospheric delay handling.

A number of least-squares processors with single-frequency code-only and code-and-carrier-phase observables were developed. Processing model hierarchy is based on measurement error handling, starting with a basic code-based navigation solution and progressing to the code-and-carrier-phase model. Measurement error handling includes receiver clock error reduction by the between-satellite differencing process, various ionospheric delay models and a tropospheric delay prediction model. Ionosphere-free results are compared against values from global ionospheric delay maps. Our current point positioning processors achieve few dm-level accuracy.

INTRODUCTION

Precise point positioning is attractive to researchers because of hardware and logistics advantages. There are other important reasons for the use of the precise point positioning technique, one of them being increased global International GPS Service (IGS) product accuracy and availability.

In order to achieve high-accuracy results, numerous research groups are using dual-frequency, geodetic-quality receiver data [Bisnath, 2004]. The UNB Geodetic Research Laboratory is presently investigating how low-cost GPS receivers might be used for precise point positioning. Some rationale for this research could be found in the results of a recent GPS community survey which indicated that low accuracy is not an obstacle to increased GNSS use, while receiver cost is [ENC GNSS Survey 2004 Results, 2004].

From the periodic review of the IGS product table, one can conclude that the IGS products have become more accurate and are being released closer to real time. Some commercial real time precise point positioning products have already been introduced by the GPS industry. On-going evaluation of these products reveals few-decimetre accuracy results [Bisnath et al., 2003].

Atmospheric error correction models became a part of the IGS product package a few years ago. A growing number of global monitoring stations and the processing power of the IGS data centres are making the IGS products more accurate and therefore a viable alternative for precise point positioning users.

FILTER MODELS AND SOLUTIONS

The vector-matrix formulations of the positioning models examined in this paper will be given in the following sub sections.

Pseudorange Model

The pseudorange-only position model, sometime referred as the navigation solution, is well documented in the Interface Control Document for GPS users (ICD-GPS-200C). The standard position solution is performed in every GPS receiver and it is shown here as an example of the "lowest accuracy solution".

The linearized filter of the pseudorange observation model is

$$\mathbf{P}_t - \mathbf{P}_t^0 = \mathbf{A}_t \delta\mathbf{x}_t + \mathbf{e}_t \; ; \mathbf{C}_{\mathbf{P}_t} \tag{1}$$

where $\mathbf{P}_t$ and $\mathbf{P}_t^0$ are the pseudorange measurement and predicted value, respectively; $\mathbf{A}_t$ measurement design matrix whose elements are the measurement partial derivatives with respect to the receiver position and clock estimates for epoch t; $\delta\mathbf{x}_t$ are the estimated corrections to the receiver position and clock at epoch t; $\mathbf{e}_t$ are the measurement errors associated with $\mathbf{P}_t$; $\mathbf{C}_{\mathbf{P}_t}$ is the covariance matrix for $\mathbf{P}_t$.

The least-squares solution for (1) is

$$\delta\mathbf{x}_t = -(\mathbf{A}_t^T \mathbf{C}_{\mathbf{P}_t}^{-1} \mathbf{A}_t^T)^{-1} \mathbf{A}_t^T \mathbf{C}_{\mathbf{P}_t}^{-1} \mathbf{w}_{\mathbf{P}_t} \tag{2}$$

where $\hat{\mathbf{x}} = \mathbf{x}^0 + \delta\mathbf{x}$ (the estimate is equal to the approximate initial value plus the estimated correction); $\mathbf{w}_{\mathbf{P}}$ is the misclosure vector for the pseudoranges.

Pseudorange Model with Between-Satellite Differences

Receiver clock error could be removed from the solution by creating between-satellite differences at each epoch. The pseudorange model with between-satellite differences was examined to investigate if the removal of the receiver clock error has any impact on horizontal and vertical position estimates.

The linearized vector–matrix equation of the between satellite filter observation model is

$$\nabla\mathbf{P}_t - \nabla\mathbf{P}_t^0 = \nabla\mathbf{A}_t \delta\mathbf{x}_t + \nabla\mathbf{e}_t \; ; \nabla\mathbf{C}_{\mathbf{P}_t} \tag{3}$$

where $\nabla\mathbf{P}_t$ and $\nabla\mathbf{P}_t^0$ are the between-satellite differenced pseudorange measurement and predicted value, respectively; $\nabla\mathbf{A}_t$ is the measurement design matrix at epoch t; $\delta\mathbf{x}_t$ are the estimated corrections to the receiver position at epoch t; $\mathbf{e}_t$ are the measurement errors associated with $\nabla\mathbf{P}_t$; $\nabla\mathbf{C}_{\mathbf{P}_t}$ is the covariance matrix for $\nabla\mathbf{P}_t$.

The solution for (3) is

$$\delta\mathbf{x}_t = -(\nabla\mathbf{A}_t^T \nabla\mathbf{C}_{\mathbf{P}_t}^{-1} \nabla\mathbf{A}_t^T)^{-1} \nabla\mathbf{A}_t^T \nabla\mathbf{C}_{\mathbf{P}_t}^{-1} \mathbf{w}_{\mathbf{P}_t} \tag{4}$$

where $\hat{\mathbf{x}} = \mathbf{x}^0 + \delta\mathbf{x}$.

Pseudorange Model - the Sequential Least Squares Solution

It is important to keep in mind that all previous models provide epoch-by-epoch independent solutions. The pseudorange model in the sequential least-squares solution is taking advantage of the previous epoch estimate and its covariance matrix. The reason why this particular model is presented here is to show the effect of smoothing in the solution domain [Kouba and Héroux, 2001].

The linearized filter observation model in matrix form is the same as that given in (1):

$$\mathbf{P}_t - \mathbf{P}_t^0 = \mathbf{A}_t \delta\mathbf{x}_t + \mathbf{e}_t \; ; \mathbf{C}_{\mathbf{P}_t} \tag{5}$$

However, the sequential least squares filter solution for (5) is

$$\delta\mathbf{x}_t = -(\mathbf{C}_{\mathbf{x}^0}^{-1} + \mathbf{A}_t^T \mathbf{C}_{\mathbf{P}_t}^{-1} \mathbf{A}_t^T)^{-1} \mathbf{A}_t^T \mathbf{C}_{\mathbf{P}_t}^{-1} \mathbf{w}_{\mathbf{P}_t}$$
$$\mathbf{C}_{\mathbf{x}^0} = \mathbf{C}_{\hat{\mathbf{x}}_{t-1}} + \mathbf{C}_{\varepsilon_{\Delta t}} \tag{6}$$

where $\hat{\mathbf{x}} = \mathbf{x}^0 + \delta\mathbf{x}$; $\mathbf{w}_{\mathbf{P}}$ is the misclosure vector for the pseudoranges; and $\mathbf{C}_{\hat{\mathbf{x}}_{t-1}}$ is the receiver position and clock covariance based on the last epoch's solution; $\mathbf{C}_{\varepsilon_{\Delta t}}$ is the process noise covariance matrix reflecting the between-epoch position change.

The process noise covariance matrix plays an important role in this type of filter. Unlike the Kalman filter process noise covariance matrix, the $\mathbf{C}_{\varepsilon_{\Delta t}}$ matrix in this filter actually dictates how much the unknown parameters could change between epochs. Choosing numerically small values for position components means that the filter assumes very little or no dynamics (appropriate for static positioning) and choosing numerically large values will result in an epoch-by-epoch independent (or kinematic) solution. Optimal results could be obtained by multiple runs of this filter and/or by some a-priori knowledge of the GPS receiver dynamics.

Pseudorange and Time-Differenced Carrier-Phase Model

The pseudorange and time differenced carrier phase model is presented here to show the fusion of pseudorange data with a factor 100 more precise time-differenced carrier phase data. Time-differenced carrier phase data also provide a connection between measurement epochs, so the actual velocity measurements (time-differenced carrier phases) provide the dynamic information to the filter [Bisnath and Langley, 2002].

The linearized pseudorange and time-differenced carrier phase filter observation model in hypermatrix form is

$$
\begin{bmatrix} \mathbf{P}_t - \mathbf{P}_t^0 \\ \boldsymbol{\delta\Phi}_t - \boldsymbol{\delta\Phi}_t^0 \end{bmatrix} = \begin{bmatrix} 0 & \mathbf{A}_t \\ -\mathbf{A}_{t-1} & \mathbf{A}_t \end{bmatrix}\begin{bmatrix} \boldsymbol{\delta x}_{t-1} \\ \boldsymbol{\delta x}_t \end{bmatrix} + \begin{bmatrix} \mathbf{e}_t \\ \boldsymbol{\varepsilon}_t \end{bmatrix};
$$
$$
\mathbf{C}_{\mathbf{P}_t}, \ \mathbf{C}_{\boldsymbol{\delta\Phi}_t},
$$

(7)

where $\mathbf{P}_t$ and $\mathbf{P}_t^0$ are the pseudorange measurement and predicted value, respectively; $\boldsymbol{\delta\Phi}_t$ and $\boldsymbol{\delta\Phi}_t^0$ are the time-differenced carrier phase measurement and predicted value, respectively; $\boldsymbol{\delta x}_{t-1}$ and $\boldsymbol{\delta x}_t$ are the estimated corrections to the receiver position and clock at epoch t-1 and t, respectively; $\mathbf{A}_{t-1}$ and $\mathbf{A}_t$ are the measurement design matrices for epochs t-1 and t, respectively; $\mathbf{e}_t$ and $\boldsymbol{\varepsilon}_t$ are the measurement errors associated with $\mathbf{P}_t$ and $\boldsymbol{\delta\Phi}_t$, respectively; $\mathbf{C}_{\mathbf{P}_t}$ and $\mathbf{C}_{\boldsymbol{\delta\Phi}_t}$ are the covariance matrices for $\mathbf{P}_t$ and $\boldsymbol{\delta\Phi}_t$, respectively. Note that at present in the model the pseudorange and carrier phase measurements are assumed uncorrelated between observables and between observations.

The best solution for (7), in a least-squares sense, is

$$
\begin{bmatrix} \hat{\mathbf{x}}_{t-1} \\ \hat{\mathbf{x}}_t \end{bmatrix}
$$
$$
= \begin{bmatrix} \mathbf{x}_{t-1}^0 \\ \mathbf{x}_t^0 \end{bmatrix} - \begin{bmatrix} \mathbf{A}_{t-1}^T \mathbf{C}_{\boldsymbol{\delta\Phi}_t}^{-1} \mathbf{A}_{t-1} + \mathbf{C}_{\hat{\mathbf{x}}_{t-1}}^{-1} & -\mathbf{A}_{t-1}^T \mathbf{C}_{\boldsymbol{\delta\Phi}_t}^{-1} \mathbf{A}_t \\ -\mathbf{A}_t^T \mathbf{C}_{\boldsymbol{\delta\Phi}_t}^{-1} \mathbf{A}_{t-1} & \mathbf{A}_t^T \left(\mathbf{C}_{\mathbf{P}_t}^{-1} + \mathbf{C}_{\boldsymbol{\delta\Phi}_t}^{-1} \right) \mathbf{A}_t \end{bmatrix}^{-1}
$$
$$
\times \begin{bmatrix} -\mathbf{A}_{t-1}^T \mathbf{C}_{\boldsymbol{\delta\Phi}_t}^{-1} \mathbf{w}_{\boldsymbol{\delta\Phi}} \\ \mathbf{A}_t^T \mathbf{C}_{\mathbf{P}_t}^{-1} \mathbf{w}_{\mathbf{P}} + \mathbf{A}_t \mathbf{C}_{\boldsymbol{\delta\Phi}_t}^{-1} \mathbf{w}_{\boldsymbol{\delta\Phi}} \end{bmatrix},
$$

(8)

where $\mathbf{w}_{\mathbf{P}}$ and $\mathbf{w}_{\boldsymbol{\delta\Phi}}$ are the misclosure vectors for the pseudoranges and time-differenced carrier phases, respectively; and $\mathbf{C}_{\hat{\mathbf{x}}_{t-1}}$ is the receiver estimated position and clock covariance matrix based on the last epoch's solution.

Tropospheric Delay Models

The typical formulation for the tropospheric delay is given as:

$$
d_{trop} = d_{hyd}^z m_{hyd} + d_{wet}^z m_{wet} \tag{9}
$$

where the total delay d_{trop} is a function of the hydrostatic zenith delay d_{hyd}^z and its mapping function m_{hyd} and the wet zenith delay d_{wet}^z and its mapping function m_{wet}.

The UNB3 tropospheric delay prediction model, which we have used in our analyses, consists of the Saastamoinen zenith tropospheric model, Neill mapping functions, surface met lookup table and height propagators. The hydrostatic component of the zenith delay can be modeled with millimetre accuracy, but the water vapour component of the tropospheric delay provides a limiting factor [Collins, 1999]. Furthermore, use of average meteorological conditions rather than the actual measurements (which is the case for the UNB3 model) introduces modelling errors on both dry and wet delays, the total zenith error of which could be in the order of 5-10 cm [Misra and Enge, 2001].

Ionospheric Delay Models

Ionospheric delay on the GPS signal is caused by the electrically charged portion of the atmosphere. The ionization of gases occurring in the Earth's atmosphere at heights from roughly 50 to 1000 km result from their interaction with the Sun's radiation. The speed of propagation of a radio signal in the ionosphere, at any instant, depends on the local electron density. The total number of free electrons (in a cross section of 1 metre squared) along the signal path is defined as the Total Electron Contend (TEC) [Misra and Enge, 2001]. In order

to nearly eliminate the effect of Earth's ionosphere for the users of GPS, a secondary frequency was incorporated into the system.

Single frequency users are provided with an algorithm, which uses 8 coefficients from the broadcast navigation message to correct for approximately 50% r.m.s. of the ionospheric range error [Klobuchar, 1987]. This Klobuchar model represents the zenith delay as a constant value at nighttime and a half-cosine function in daytime with a maximum at 2 pm local time. Update of the Klobuchar model coefficients occurs when there is a significant change in the 10.7 cm solar flux.

Using global IGS station data (geometry-free linear combination which carries ionospheric delay data), the Center for Orbit Determination in Europe (CODE) computes global ionosphere maps. TEC is developed into a series of spherical harmonics adopting a single-layer model in a Sun-fixed reference frame. Each day, a set of TEC coefficients, which approximates an average distribution of vertical TEC within a certain time interval on a global grid, is computed.

The Ionosphere Map Exchange Format (IONEX) supports the exchange of 2-dimensional or 3-dimensional TEC maps in a geographic grid [Schaer and Guntner, 1998]. Maps are epoch specific. Procedures to compute the TEC value as a function of geodetic latitude, longitude and universal time are described in Schaer [1997]. The CODE recommended strategy is to interpolate between consecutive TEC maps by $t - T_i$ (where t is the interpolation time and T_i is the map reference epoch time) rotated around the Z-axis to compensate for the strong correlation between the ionosphere and the Sun's position.

DATA TESTING AND ANALYSIS

The data from Algonquin IGS station (ALGO) were used in all tests except the one with pseudorange and time-differenced carrier phase model. A 24-hour dataset with 30 s sampling interval from July 17, 2004 was used. ALGO is equipped with an AOA BenchMark ACT GPS receiver with the AOAD/M_T choke ring antenna and a hydrogen maser clock. A 10 degree elevation angle cut-off was applied to the data.

For the test of the pseudorange and time-differenced carrier phase model, 12 and 4-hour datasets with 1 s sampling interval from the high-rate Halifax IGS station (HLFX) from July 17, 2004 were used. HLFX is equipped with an AOA BenchMark ACT GPS receiver and with the AOAD/M_B choke ring antenna and a rubidium clock. A 10 degree elevation angle cut-off was applied to the data.

IGS computes weekly cartesian coordinates of all IGS reference stations. The coordinates for the Algonquin station were obtained from the IGS final solution for the week 1279. Halifax station reference coordinates were not found in this solution, and so the coordinates from the California Spatial Reference System (CSRS) for week 1234 were used instead.

Atmospheric Model Testing

The performance of the pseudorange model without atmospheric correction models, and the pseudorange model with the UNB3 tropospheric delay model and the Kobuchar ionospheric delay model will be compared in the first part. The pseudorange model with the UNB3 tropospheric delay model and TEC-map-derived ionospheric delay corrections and the ionosphere-free pseudorange model with the UNB3 tropospheric delay model will be compared in the second part.

Pseudorange Model with and without Atmospheric Correction Models

The UNB3 tropospheric delay prediction model and the Klobuchar ionospheric model were switched on and off in the software to demonstrate the impact on the positioning results. The first set of plots (Figure 1) shows the north, east, up and the receiver clock error time series estimated by the pseudorange model without any atmospheric error corrections. The r.m.s. of the residuals is 1.31 m, but the up-component shows a very large bias as expected.
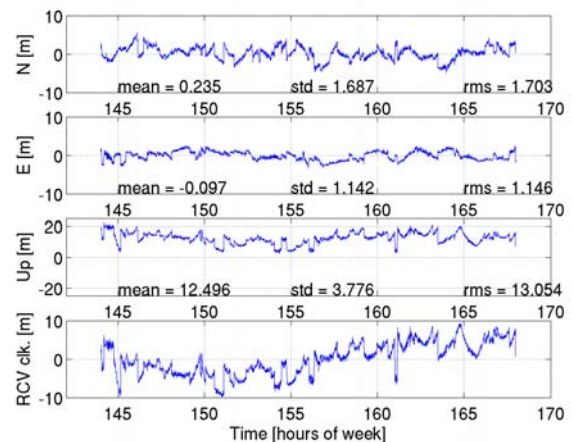

Figure 1: Position component and receiver clock errors of the pseudorange model without any atmospheric error corrections.

The second set of plots (Figure 2) shows the positioning results from the same functional model with the UNB3 tropospheric delay model and the broadcast ionospheric delay model enabled. The result of this experiment is a decrease in up component bias, from 12.50 m to –1.63 m. The r.m.s. of the residuals corresponding to these results

is 1.09 m, which is about 2 dm lower than those related to Figure 1.
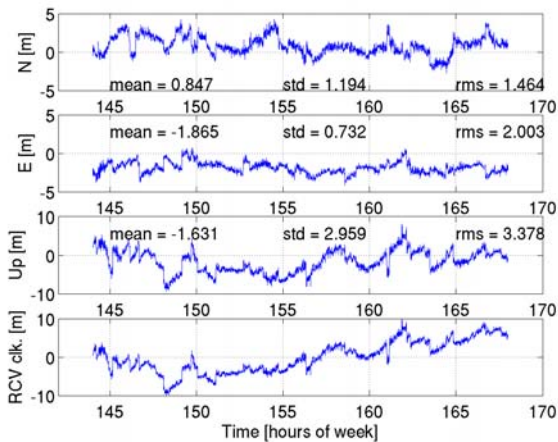

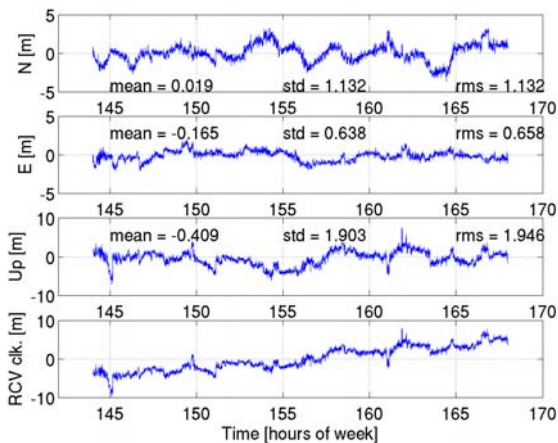
Figure 2: Position component and receiver clock errors of the pseudorange model with UNB3 tropospheric delay model and broadcast ionospheric delay model.

Pseudorange Model with Broadcast Ionospheric Model vs. Pseudorange Model with Global TEC Map Ionospheric Model

A important part of the research described in this paper is the handling of the ionospheric delay. Results plotted in Figure 2 indicate the capabilities of the broadcast ionospheric model. It is expected that the broadcast ionospheric model will correct for at least 50% of the ionospheric delay. The next set of plots (Figure 3) shows the results of the pseudorange model with the UNB3 tropospheric delay model and the global TEC map ionospheric delay model.

Figure 3: Position component and receiver clock errors of the pseudorange model with UNB3 tropospheric delay model and global TEC map ionospheric delay model.

The global TEC map includes r.m.s. values for the vertical TEC estimates. The r.m.s. values on the TEC map used indicate decimetre-level vertical residual ionospheric biases. Filter residuals shown in Figure 4 indicate the

presence of unmodelled errors (r.m.s. of the pseudorange residuals from this filter are 0.925 m). Overall the up-component bias went down in magnitude from −1.63 m to −0.41 m.
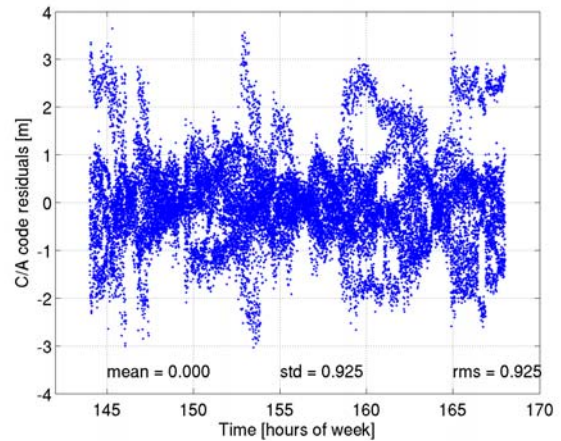

Figure 4: Filter residuals from the pseudorange model with UNB3 tropospheric delay model and global TEC map ionospheric delay model.

Pseudorange Model with Global TEC Map Ionospheric Model and Ionosphere-Free Pseudorange Model

The ionospheric delay effect can be nearly eliminated if the measurements from both GPS signal frequencies are combined in a linear combination, known as the ionosphere-free linear combination. Although our interest lies in assessing single-frequency capability, we have examined the ionosphere-free combination as a benchmark solution. This linear combination was used as an input to the pseudorange model (with the UNB3 tropospheric delay model still included) to show the results, which are not affected by the ionospheric delay (Figure 5).
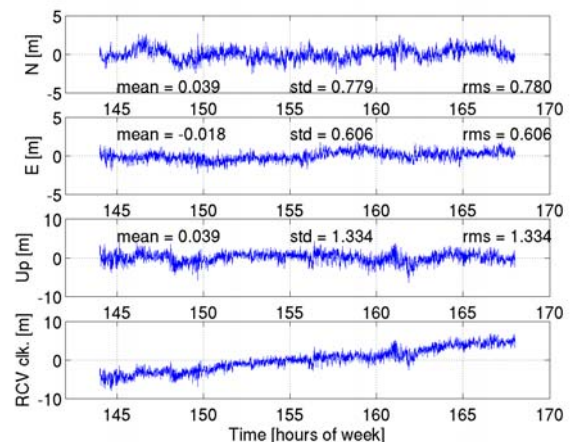

Figure 5: Position component and receiver clock errors of the ionosphere-free pseudorange model with the UNB3 tropospheric delay model.
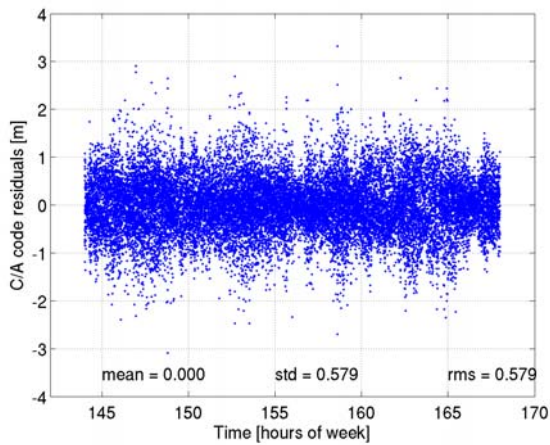
Figure 6: Filter residuals from the ionosphere-free pseudorange model with the UNB3 tropospheric delay model

Although the ionosphere bias is removed, the use of the ionosphere-free linear combination has a drawback in the increase of measurement noise by a factor of approximately three. The up-component bias in the single-frequency results displayed in Figure 3 is –0.41 m while that of the ionosphere-free results in Figure 5 is 0.04 m. The residuals of the ionosphere-free pseudorange model with the UNB3 tropospheric delay model are plotted on Figure 6. The r.m.s. of the residuals is 0.58 m.

Testing of Functional and Stochastic Models

The three following sub-sections will justify the selection of various functional and stochastic models and error correction models.

Pseudorange Model vs. Pseudorange Model with Between-Satellite Differences

The pseudorange model with between-satellite differences was examined to investigate if the removal of the receiver clock error has any impact on horizontal and vertical position estimates. Figure 3 presented the results generated by the pseudorange model with the UNB3 tropospheric delay model and with the global TEC map ionospheric delay model. 3D bias is 0.44 m, 3D r.m.s. is 2.30 m, and r.m.s. of the residuals is 0.93 m.

Figure 7 presents the results from the pseudorange model with between-satellite differences using the same atmospheric delay models. The r.m.s. of the residuals from this model is 1.22 m. One disadvantage of this model is the lower number of observations at any given epoch due to between-satellite differencing. Position component statistics shown in Figure 7 are slightly worse than those in Figure 3. 3D bias is 0.89 m, 3D r.m.s. is 2.96 m.

The clock estimates in Figure 3 might be soaking up some of the residual atmosphere error. That is not possible in the Figure 7 approach. Repeating Figure 7 analysis with the ionosphere-free data might show results closer to those of Figure 5 but the tropospheric delay residual will still be a factor.
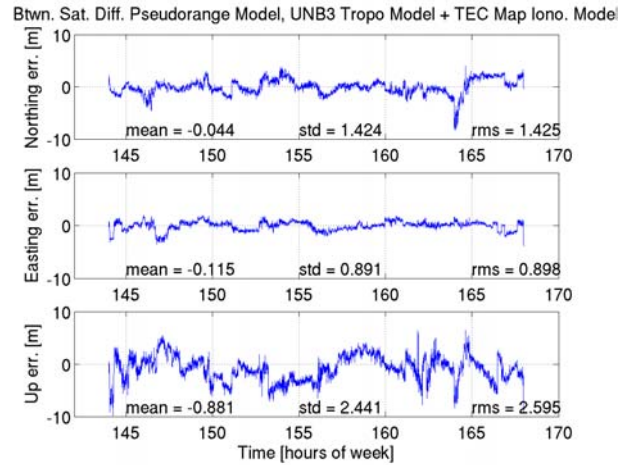

Figure 7: Position component and receiver clock errors of the pseudorange model with between-satellite differences.

Pseudorange Model vs. Pseudorange Model - the Sequential Least Squares Solution

The pseudorange model with the UNB3 tropospheric delay model and with the global TEC map ionospheric delay model (Figure 3) is an example of epoch-by-epoch processing. The pseudorange model with a sequential least-squares solution produces results (Figure 8) which are smoother (standard deviations of the horizontal and vertical components in Figure 8 are 1 dm and 2 dm smaller, respectively than those in Figure 3).
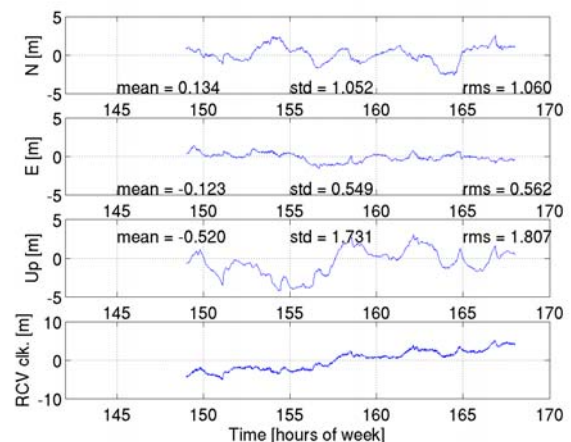

Figure 8: Position component and receiver clock errors of the pseudorange model with the sequential least-squares solution without the initial convergence period.

The filtering in the solution domain depends to a large extent on the matrix reflecting the between-epoch position

and receiver clock change. Process noise variance for position components was 10^{-2} m²/epoch and 10^{-8} m²/epoch for the receiver clock error estimates. The receiver clock process noise variance is a couple orders of magnitude larger than the short-term stability of the hydrogen maser so the clock term can absorb a portion of unmodelled atmospheric biases. 3D bias is 0.46 m, 3D r.m.s. is 1.97 m. and the r.m.s. of the residuals from this filter is 0.96 m.

Pseudorange Model - the Sequential Least Squares Solution vs. Pseudorange and Time-Differenced Carrier-Phase Model

All functional models tested above used only pseudorange observations. The sequential least-squares solution, shown in Figure 8, represents the upper limits of accuracy of pseudorange data processing. The accuracy of the results in Figure 8 is similar to those from the epoch-by-epoch solution shown in Figure 3, but the standard deviations of the position components in Figure 8 are about 1 dm smaller than those in Figure 3.

High-precision point positioning models use carrier-phase observations in many different ways. The pseudorange and time-differenced carrier-phase model was chosen to represent the high-precision point positioning models, because of its independence from platform dynamics. It was discovered that this filter does not work well with the 30 s sampling interval data, because the unmodelled errors in the time-differenced carrier-phase observations tend to grow larger over 30 s sampling interval than they would with 1 s sampling interval. 1 s sampling interval datasets from station HLFX were used instead of the 30 s sampling interval ALGO data.
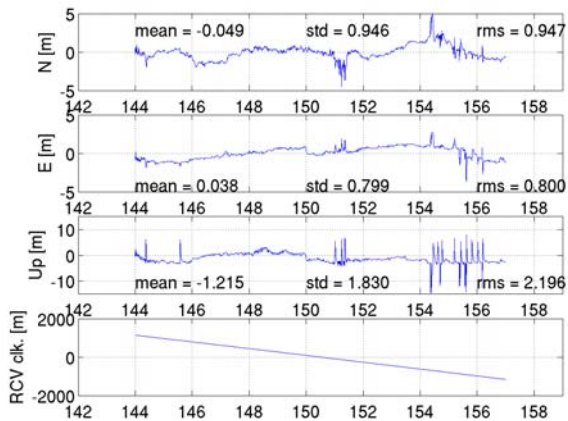

Figure 9: Position component and receiver clock errors of the pseudorange and time-differenced carrier phase model for the 13-hour data period.

The first set of plots (Figure 9) in this section shows the results of pseudorange and time-differenced carrier phase filter processing 13 hours of the HLFX dataset. The 3D

bias as well as the r.m.s. of the code and phase residuals are quite high, due to uncorrected cycle slips in the data, which resulted, e.g., in spikes in the up component time-series. A four-hour cycle-slip-free portion of the HLFX data was processed separately.
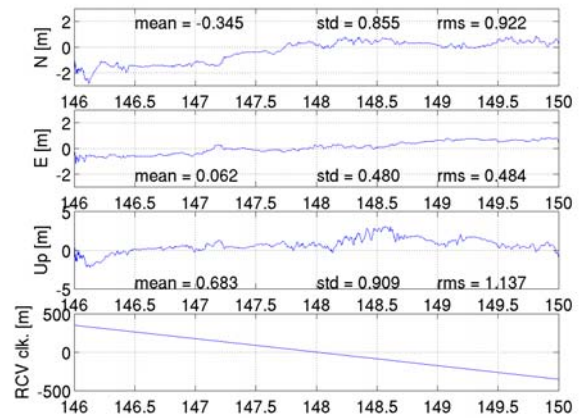

Figure 10: Pseudorange and time-differenced carrier phase model. 4 hour cycle-slip-free period.

The results from this smaller dataset are displayed in Figure 10. The 3D bias is about 0.8 m in this case. Pseudorange residuals from the pseudorange and time-differenced carrier phase model are displayed in Figure 11 and the time-differenced carrier-phase residuals are displayed in Figure 12. The pseudorange residuals show that there is a bias in the solution due to unmodelled biases. Outliers in the time differenced carrier-phase residuals just before hour 148 (Figure 12) remain to be investigated.
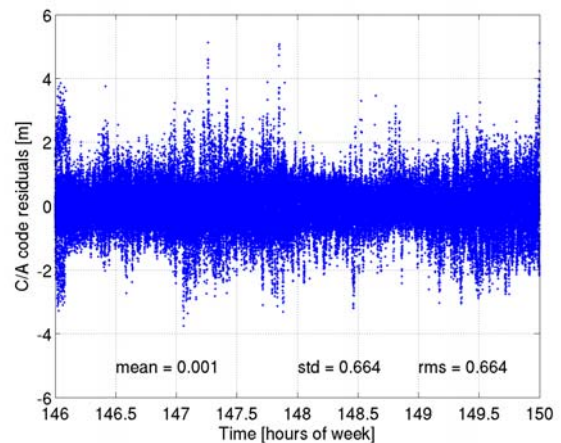

Figure 11: Pseudorange residuals from the pseudorange and time-differenced carrier phase model (4 hour dataset).
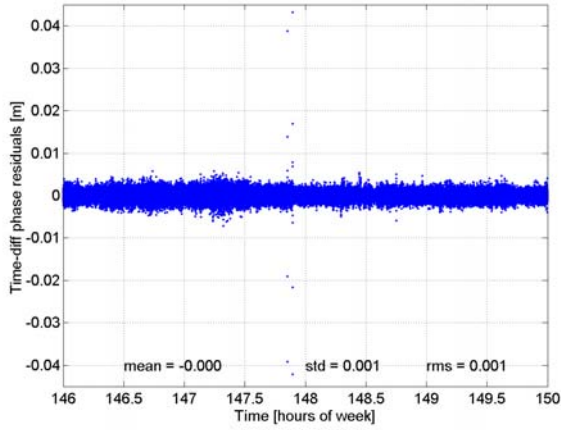
Figure 12: Time-differenced carrier-phase residuals from the pseudorange and time-differenced carrier phase model (4 hour dataset).

SUMMARY AND CONCLUSIONS

The effect of atmospheric correction models on the solution were examined in the first part of this paper. The primary objective of this research was ionospheric error handling, so the resulting statistics refer to the pseudorange models using broadcast TEC, map-generated ionospheric models, and the ionosphere-free results (Table 1).

Iono. Delay Model	3D Bias [m]	r.m.s. of the code residuals [m]
Klobuchar	2.62	1.09
TEC Map	0.44	0.93
Ionosphere-free	0.06	0.58

Table 1: 3D bias and r.m.s. of the residuals of different ionospheric delay models used in the same pseudorange model solutions (all solutions include UNB3 tropospheric delay model).

The use of different functional and stochastic models are summarized in the second table. The pseudorange model, the pseudorange model with between-satellite differences, the sequential least-squares solution and the pseudorange and time-differenced carrier-phase 3D bias and r.m.s. are used in the comparison.

From the testing of atmospheric correction models, the following conclusions were made. The UNB3 tropospheric delay model helps reduce the bias in the up-component. Many solution discontinuities also disappeared. The Klobuchar-model-derived corrections for the ionospheric models are not as good as the TEC-map-derived corrections. The residual ionospheric delay errors from the TEC-map-derived corrections are still causing about a 4 dm bias in the up component. The ionosphere-free solution is better than the TEC map

solution as expected. The 3D bias from this solution is less than 1 dm.

Functional Model	3D Bias [m]	r.m.s. of the code (and phase) residuals [m]
Pseudorange model with. btwn. sat. diff.	0.89	1.22
Pseudorange model	0.44	0.93
Sequential LS solution	0.55	0.96
Pseudorange and time-diff. carrier-phase model	0.76	0.66 (0.001)

Table 2: 3D bias and r.m.s. of residuals of different functional and stochastic models.

Use of between-satellite differences in the pseudorange model removes the receiver clock error from the solution. The decrease geometrical strength (see e.g., Vaníček et al. [1984]) and lower number of observations are partially responsible for the results being worse than those of the original pseudorange model. The main reason why the results of the between-satellite difference model are worse is the fact that in the basic pseudorange approach, the receiver clock error parameter is absorbing some of the unmodelled biases (e.g., residual ionospheric and tropospheric delay). It could be concluded that if the receiver clock error parameter gets eliminated from the solution, the unmodelled biases get absorbed to a certain degree by the other estimated parameters.

The sequential-least squares solution gives optimal results, if a realistic process noise covariance matrix is chosen. The direct result of the smoothing in the solution domain could be seen when standard deviations of the position components are compared.

High sampling rate data was needed for the pseudorange and time-differenced carrier-phase model, because the unmodelled biases in the time-difference carrier-phase observations grow too much over a 30 s interval. Cycle slips in the solution need to be filtered.

FURTHER RESEARCH

Residual atmospheric delay estimation is needed to further improve the results. A residual zenith atmospheric delay parameter will be added to the solution. A cycle-slip detection algorithm in the form of statistical residual outlier testing should be implemented. There are some point-positioning-specific correction models which remain to be considered, e.g., GPS satellite centre of mass – antenna phase centre offset for the IGS orbits, carrier-phase windup, and for terrestrial datasets, Earth tides and ocean loading effects should be modelled. Multipath

handling is another significant concern, because of the long-term focus on low-cost GPS receivers and lower-quality data in this research. A multipath stochastic modelling approach will be implemented.

ACKNOWLEDGEMENTS

REFERENCES

Bisnath, S.B. and R.B. Langley (2002). "High-Precision, Kinematic Positioning with a Single GPS Receiver." *NAVIGATION: Journal of the Institute of Navigation*, Vol. 49, No. 3, Fall 2002, The Institute of Navigation, Alexandria, Virginia, U.S.A., pp. 161-169.

Bisnath S.B., D. Wells, and D. Dodd (2003). "Evaluation of Commercial Carrier-Phase-Based WADGPS Services for Marine Applications." *Proceedings of the 16th International Technical Meeting of the Satellite Division of The Institute of Navigation*, Portland, Oregon, U.S.A., 9-12 September, 2003, The Institute of Navigation, Alexandria, Virginia, U.S.A., pp. 17-27.

Bisnath, S.B. (2004). *Precise Orbit Determination of Low Earth Orbiters with a Single GPS Receiver-Based, Geometric Strategy.* Ph.D. Dissertation, Department of Geodesy and Geomatics Engineering Technical Report No. 220, University of New Brunswick, Canada, 143 pp.

Collins, J.P. (1999). *Assessment and Development of the Tropospheric Delay Model for Aircraft Users of the Global Positioning System.* M.Sc.E. Thesis, Department of Geodesy and Geomatics Engineering Technical Report No. 203, University of New Brunswick, Canada, 174 pp.

ENC GNSS Survey 2004 Results http://www.rin.org.uk/SITE/UPLOAD/DOCUMENT /GNSS2004survey.pdf

Hilla, S. and G. Adams (2001). "C++ Classes for Reading and Writing RINEX Files." *GPS Solutions*, Vol. 5, No.1, pp. 65-67; Vol. 5, No.2, pp. 87-89.

ICD-GPS-200C(1999). *Navstar GPS Space Segment/Navigation User Interface Control Document*. ARINC Research Corporation, 138 pp.

Klobuchar, J.A. (1987). "Ionospheric Time Delay Algorithm for Single Frequency GPS Users." *IEEE Transactions on Aerospace and Electronic Systems*, Vol. AES-23, No. 3, pp. 325-331.

Kouba, J. and P. Héroux (2001). "Precise Point Positioning Using IGS Orbit and Clock Products." *GPS Solutions*, Vol. 5, No. 2, pp.12-28.

Misra, P. and P. Enge (2001) *Global Positioning System: Signals, Measurements, and Performance.* Ganga-Januma Press, Lincoln, Massattchusetts, 390 pp.

Schaer, S. (1997). "How to Use CODE's Global Ionosphere Maps." Astronomical Institute, University of Berne, Switzerland, (http://www.aiub.unibe.ch/ionosphere/gimman.pdf).

Schaer, S., W. Guntner, and J.Feltens (1998). "IONEX: The IONosphere Map Exchange Format Version 1." *Proceedings of the IGS AC Workshop*, Darmstadt, Germany, February 9-11, 1998, pp. 233-237.

Vaníček P., R.B. Langley, D.E. Wells, D. Delikaraoglou (1984). "Geometrical Aspects of Differential GPS Positioning." *Bulletin Géodésique*, Vol. 58, pp. 37-52.